Vol 11 No 4, April 2002
1009-1963/2002/11(04)/0366-09

Chinese Physics

Non-equilibrium extrapolation method for velocity and pressure boundary conditions in the lattice Boltzmann method*

Guo Zhao-Li(郭照立)[a], Zheng Chu-Guang(郑楚光)[a], and Shi Bao-Chang(施保昌)[b]

[a] *National Laboratory of Coal Combustion, Huazhong University of Science and Technology, Wuhan* 430074, *China*

[b] *Department of Mathematics, Huazhong University of Science and Shenyang* 110023, *China*

(Received 1 September 2001; revised manuscript received 12 October 2001)

In this paper, we propose a new approach to implementing boundary conditions in the lattice Boltzmann method (LBM). The basic idea is to decompose the distribution function at the boundary node into its equilibrium and non-equilibrium parts, and then to approximate the non-equilibrium part with a first-order extrapolation of the non-equilibrium part of the distribution at the neighbouring fluid node. Schemes for velocity and pressure boundary conditions are constructed based on this method. The resulting schemes are of second-order accuracy. Numerical tests show that the numerical solutions of the LBM together with the present boundary schemes are in excellent agreement with the analytical solutions. Second-order convergence is also verified from the results. It is also found that the numerical stability of the present schemes is much better than that of the original extrapolation schemes proposed by Chen *et al.* (1996 Phys. Fluids **8** 2527).

Keywords: Lattice Boltzmann method, Boundary conditions
PACC: 5100, 4700, 0270

1. Introduction

The lattice Boltzmann method (LBM) is a new technique for simulating fluid flows and modelling complex physics in fluids. In the last decade, the LBM has achieved great success in a variety of fields, ranging from simple laminar flows to thermal flows,[2,3] high-speed compressible flows,[1,4] multiphase flows,[5,6] and so on. Interested readers can see the comprehensive reviews of this method.[7,8] In the LBM, the boundary conditions play important roles in that they influence the accuracy and stability of the method.[9,10] The boundary condition most commonly used in the LBM is the bounce-back method, which originates from the lattice gas automata.[11,12] The bounce-back scheme is easy to implement and supports the idea that the LBM is ideal for simulating fluid flows in complicated geometries.[8] However, it was found that the bounce-back scheme is only of first-order in numerical accuracy at the boundaries, which is not consistent with the order of the LBM in interior points.[13] An additional disadvantage of the bounce-back scheme is that it cannot be simply extended to handle moving boundaries or mass injection through the boundaries.[14]

Some other methods have been proposed to improve the numerical accuracy of the LBM. Ziegler[12] noticed that if the boundary is shifted into the fluid by one half mesh unit, the bounce-back scheme is of second order. Skordos *et al.*[15] proposed the use of a new equilibrium distribution function, which includes velocity gradients at the boundaries. Noble *et al.*[14] proposed a consistent hydrodynamic boundary condition, which calculates the distribution functions at the boundaries from the velocity boundary conditions and the distributions of neighbouring fluid nodes at the boundary. Maier *et al.*[16] generalized the hydrodynamic method by introducing some supplementary rules. Inamuro *et al.*[17] proposed a non-slip boundary condition, where the unknown distributions at the wall are assumed to be an equilibrium distribution with a counter slip velocity which is to be determined so that the wall conditions are satisfied. Zou *et al.*[10] proposed a way to specify pressure and velocity boundary conditions based on the idea of bounce back of the non-equilibrium part of the distribution.

*Project supported by the Special Funds for Major State Basic Research Programmes (Grant No G1999022207) and by the National Natural Science Foundation of China (Grant No 6073044).

The boundary treatments mentioned above can yield improved accuracy compared to the bounce-back scheme. However, it is difficult to extend them to arbitrary boundary conditions. Chen *et al.*[18] noticed that the LBM can be viewed as a special finite difference scheme of the Boltzmann equation, and proposed the use of a second-order extrapolation scheme of distributions in the fluid to obtain the unknown distributions. This extrapolation scheme is simple and can be extended to include velocity, temperature, and pressure boundary conditions and their derivatives. Unfortunately, the numerical stability of the extrapolation scheme was found to be unsatisfactory.[10,18]

It is common knowledge that the lower-order extrapolation is usually more stable than the higher-order extrapolation. Therefore, if we adopt a first-order extrapolation scheme to determine the unknown distributions at the boundaries, the LBM is expected to have better stability. Unfortunately, if such a first-order extrapolation scheme is applied directly to the distribution function, the resulting scheme will also be of first order. In this paper, from the finite-difference viewpoint of the LBM, and motivated by the idea used by Zou *et al.*,[10] namely the bounce back of the non-equilibrium part of the distribution, we propose a new extrapolation method for boundary conditions in the LBM. The basic idea is to use a first-order extrapolation scheme of the non-equilibrium part of the distributions in the fluid to obtain the unknown distributions at the boundaries. To evaluate the accuracy and stability of the present non-equilibrium extrapolation schemes, numerical tests including two-dimensional Poiseuille flow, porous plate flow, oscillating plate flow and driven cavity flow are carried out, and the simulation results are analysed in detail.

2. The lattice Boltzmann method

The lattice Boltzmann model used in this study is the nine-velocity incompressible lattice Bhatnagar–Gross–Krook model (ID2Q9) proposed by the present authors.[19] The ID2Q9 can model the incompressible Navier–Stokes equation correctly. The directions of the discrete velocity used in the model are given by $\mathbf{e}_0 = 0$, $\mathbf{e}_i = (\cos[(i-1)\pi/2], \sin[(i-1)\pi/2])$ for $i = 1:4$, and $\mathbf{e}_i = \sqrt{2}(\cos[(i-5)\pi/2+\pi/4], \sin[(i-5)\pi/2+\pi/4])$ for $i = 5:8$. The evolution equation of the distribution function $g_i(x,t)$ reads

$$g_i(\mathbf{x}+c\mathbf{e}_i\triangle t, t+\triangle t) - g_i(\mathbf{x},t) = -\frac{1}{\tau}[g_i(\mathbf{x},t) - g_i^{(0)}(\mathbf{x},t)], \quad (1)$$

where $c = \triangle x/\triangle t$ is the particle speed, $\triangle x$ and $\triangle t$ are the lattice spacing and the time step, respectively. τ is the dimensionless relaxation time. $g_i^{(0)}(x,t)$ is the equilibrium distribution function defined by

$$g_i^{(0)} = \alpha_i p + \omega_i\left[3\frac{(\mathbf{e}_i\cdot\mathbf{u})}{c} + 4.5\frac{(\mathbf{e}_i\cdot\mathbf{u})^2}{c^2} - 1.5\frac{|\mathbf{u}|^2}{c^2}\right], \quad (2)$$

where $\omega_0 = 4/9$, $\omega_i = 1/9$ for $i = 1:4$, and $\omega_i = 1/36$ for $i = 5:8$. $\alpha_0 = -4\sigma/c^2$, $\alpha_i = \lambda/c^2$ for $i = 1:4$, and $\alpha_i = \gamma/c^2$ for $i = 5:8$. σ, λ and γ are parameters satisfying $\lambda+\gamma = \sigma, \lambda+2\gamma = 1/2$.

The flow velocity and pressure are given by

$$\mathbf{u} = \sum_{i=1}^{8} c\mathbf{e}_i g_i, \quad p = \frac{c^2}{4\sigma}\left[\sum_{i=1}^{8} g_i - \frac{2}{3}\frac{|\mathbf{u}|^2}{c^2}\right]. \quad (3)$$

Through multi-scaling expansion, and neglecting the terms of $O(\epsilon M^2)$ ($M \approx |\mathbf{u}|/c$ is the Mach number), the incompressible Navier–Stokes equations can be derived correctly from this incompressible ID2Q9 model as[19]

$$\nabla\cdot\mathbf{u} = 0, \quad (4)$$

$$\frac{\partial\mathbf{u}}{\partial t} + \mathbf{u}\cdot\nabla\mathbf{u} = -\nabla p + \nu\nabla^2\mathbf{u}, \quad (5)$$

to the order of $O(\epsilon^2)$, where $\epsilon = \triangle t$, and the kinetic viscosity ν is determined by

$$\nu = \frac{(2\tau-1)}{6}\frac{(\triangle x)^2}{\triangle t}. \quad (6)$$

3. Non-equilibrium extrapolation method

In hydrodynamic problems, the boundary condition is usually given for macroscopic variables, such as velocity and pressure. But in the lattice Boltzmann method, the basic evolution variable is the distribution function g_i, which is usually not given directly at the boundaries. Therefore, one must choose an appropriate method to determine the distribution function at the boundaries from the given macroscopic variables.

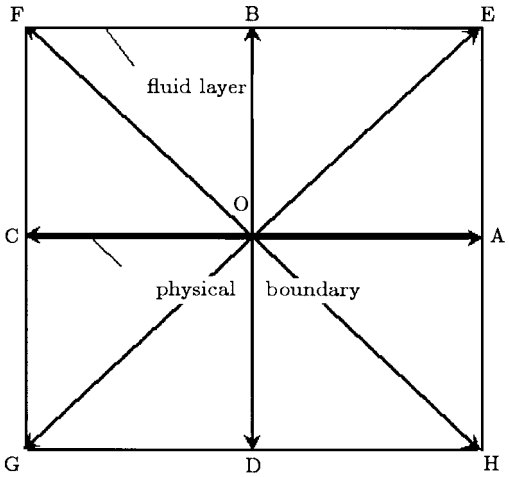

Fig.1. A boundary node and its neighbours.

It has been shown that LBM can be viewed as a special finite-difference scheme for the Boltzmann equation of a lattice,[18] and based on this idea, Chen *et al.*[18] has proposed an extrapolation scheme for boundary conditions in the LBM. Also, based on this viewpoint and based on the idea of extrapolating the non-equilibrium part of the distribution, we propose a new extrapolation method to implement velocity and pressure boundary conditions. For illustration and simplicity, we consider the case of a flat boundary. As shown in Fig.1, the COA line lies at the boundary, the nodes F, B and E are those lying in the fluid, and G, D and H are the nodes outside the fluid.

Note that one evolution equation of the LBM, Eq.(1), consists of two computational steps

$$\begin{aligned} &\text{collision:} \quad g_i^+(\mathbf{x},t) = (1-\omega)\, g_i(\mathbf{x},t) + \omega g_i^{(0)}(\mathbf{x},t), \\ &\text{streaming:} \quad g_i(\mathbf{x}+c\mathbf{e}_i\Delta t, t+\Delta t) = g_i^+(\mathbf{x},t), \end{aligned} \tag{7}$$

where $\omega = 1/\tau$. Obviously, $g_i^+(\mathrm{O},t)$ is needed to finish the streaming step for $i = 2$, 5 and 6 at the boundary node O. Notice that the distribution function $g_i(\mathbf{x},t)$ can be decomposed into its equilibrium and non-equilibrium parts

$$g_i(\mathbf{x},t) = g_i^{(0)}(\mathbf{x},t) + g_i^{(ne)}(\mathbf{x},t), \tag{8}$$

where $g_i^{(0)}$ and $g_i^{(ne)}$ are equilibrium and non-equilibrium parts of g_i, respectively. Thus the post-collision distribution function at the boundary node, $g_i^+(\mathrm{O},t)$, can be rewritten as

$$g_i^+(\mathrm{O},t) = g_i^{(0)}(\mathrm{O},t) + (1-\omega)\, g_i(^{(ne)}(\mathrm{O},t). \tag{9}$$

First we discuss how to calculate the non-equilibrium part $g_i^{(ne)}$. As in the Chapman–Enskog analysis for the lattice Boltzmann method, we assume that $g_i^{(ne)} = \epsilon g_i^{(1)}$. Note that, at time t, the macroscopic velocity and pressure of the flow is known at the fluid node B, so $g_i^{(0)}(B,t)$ can be determined, and thus the non-equilibrium part of the distribution at node B can be given by

$$g_i^{(ne)}(B,t) = g_i(B,t) - g_i^{(0)}(B,t). \tag{10}$$

Also note that node B is a neighbour of node O at a distance $\Delta x = c\epsilon$, hence $g_i^{(1)}(\mathrm{O},t) = g_i^{(1)}(B,t) + \mathrm{O}(\epsilon)$, and $g_i^{(ne)}(\mathrm{O},t)$ can be approximated by a first-order extrapolation

$$g_i^{(ne)}(\mathrm{O},t) = g_i(B,t) - g_i^{(0)}(B,t) + \mathrm{O}(\epsilon^2). \tag{11}$$

Equation (11) implies that the accuracy of the approximation of $g_i^{(ne)}(\mathrm{O},t)$ with the first-order extrapolation scheme based on $g_i^{(ne)}(B,t)$ is indeed of second order.

Now we discuss how to determine the equilibrium part $g_i^{(0)}(\mathrm{O},t)$ according to pressure and velocity boundary conditions. For the pressure boundary condition where the pressure $p(\mathrm{O},t)$ is known and velocity $\mathbf{u}$ is unknown, we approximate $g_i^{(0)}$ with a modified equilibrium $\overline{g}_i^{(0)}(\mathrm{O},t)$, defined by

$$\overline{g}_i^{(0)}(\mathrm{O},t) = \alpha_i p(\mathrm{O},t) + s_i\left(\mathbf{u}(B,t)\right), \tag{12}$$

where

$$s_i(\mathbf{u}) = \omega_i \left[3\frac{(\mathbf{e}_i\cdot\mathbf{u})}{c} + 4.5\frac{(\mathbf{e}_i\cdot\mathbf{u})^2}{c^2} - 1.5\frac{|\mathbf{u}|^2}{c^2} \right]. \tag{13}$$

For the velocity condition where $\mathbf{u}(\mathrm{O},t)$ is known and $p(\mathrm{O},t)$ is unknown, we approximate $g_i^{(0)}(\mathrm{O},t)$ with another modified equilibrium $\overline{\overline{g}}_i^{(0)}(\mathrm{O},t)$, defined by

$$\overline{\overline{g}}_i^{(0)}(\mathrm{O},t) = \alpha_i p(B,t) + s_0\left(\mathbf{u}(\mathrm{O},t)\right). \tag{14}$$

Note that $\mathbf{u}(B,t) - \mathbf{u}(\mathrm{O},t) = (\mathbf{e}_2\cdot\nabla\mathbf{u})\triangle x = \mathrm{O}(\epsilon M)$, and $p(B,t) - p(\mathrm{O},t) = (\mathbf{e}_2\cdot\nabla p)\triangle x = \mathrm{O}(\epsilon M^2)$, so we have

$$g_i^{(0)}(\mathrm{O},t) = \overline{g}_i^{(0)}(\mathrm{O},t) + \mathrm{O}(\epsilon M), \tag{15}$$

$$g_i^{(0)}(\mathrm{O},t) = \overline{\overline{g}}_i^{(0)}(\mathrm{O},t) + \mathrm{O}(\epsilon M^2). \tag{16}$$

From Eq.(6), we can obtain

$$M \approx u_0/c = \left(\tau - \frac{1}{2}\right)\frac{Re}{3L}\triangle x, \tag{17}$$

where u_0 and L are the characteristic velocity and length, respectively, and Re is the Reynolds number. If τ is chosen such that $(\tau - 0.5)Re/L = \mathrm{O}(1)$, the

Mach number will be of the same order of ϵ, and so from Eqs.(15) and (16) we have

$$g_i^{(0)}(\mathrm{O},t) = \overline{g}_i^{(0)}(\mathrm{O},t) + \mathrm{O}(\epsilon^2), \tag{18}$$

$$g_i^{(0)}(\mathrm{O},t) = \overline{\overline{g}}_i^{(0)}(\mathrm{O},t) + \mathrm{O}(\epsilon^3). \tag{19}$$

That is to say, the approximation of $g_i^{(0)}(\mathrm{O},t)$ with $\overline{g}_i^{(0)}(\mathrm{O},t)$ or $\overline{\overline{g}}_i^{(0)}(\mathrm{O},t)$ is at least of a second-order accuracy.

Summing up the above discussion, we can obtain the following non-equilibrium extrapolation schemes for boundary conditions in the ID2Q9 model: (i) for the pressure boundary condition, the distributions at the boundary node are given by

$$g_i(\mathrm{O},t) = \overline{g}_i^{(0)}(\mathrm{O},t) + (1-w)[g_i(B,t) - g_i^{(0)}(B,t)], \tag{20}$$

and (ii) for the velocity boundary condition, the distributions at the boundary node are given by

$$g_i(\mathrm{O},t) = \overline{\overline{g}}_i^{(0)}(\mathrm{O},t) + (1-w)[g_i(B,t) - g_i^{(0)}(B,t)]. \tag{21}$$

From the arguments given above, we can conclude that the two boundary conditions are both of second-order accuracy, which is consistent with the accuracy of the ID2Q9 model. Furthermore, since only first-order extrapolations are used, both schemes are expected to have better stability than that proposed in Ref.[18]. Schemes for other boundary conditions can also be designed in a similar manner.

4. Numerical results

To evaluate the accuracy and stability of the proposed non-equilibrium extrapolation schemes for pressure and velocity boundary conditions in the ID2Q9 model, numerical tests including the steady Poiseuille flow, the porous plate flow, the unsteady oscillating plate flow, and the driven cavity flow, are carried out using the present schemes for boundary conditions. In simulations, unless mentioned otherwise, the value of the relaxation parameter ω is taken to be 0.9, 1.1 and 1.7; and for each value of ω, the lattice spacing Δx ranges from 1/10 to 1/80.

4.1. Poiseuille flow

The Poiseuille flow driven by a constant pressure gradient is defined in the region $0 \le x \le 2$ and $0 \le y \le 1$. The profile of the analytical velocity is expressed as a parabola centred around the axis of the channel

$$u = u_0 y(1-y), \quad v_e = 0, \quad p = p_{in} - \frac{\Delta p}{2}x, \tag{22}$$

where $u_0 = \Delta p/16\nu$ is the centreline velocity, $\Delta p = p_{in} - p_{out}$ is the pressure drop, and p_{in} and p_{out} are the constant pressures maintained at the inlet and outlet of the channel, respectively.

The Reynolds number of the flow is defined by $Re = u_0/\nu$. In simulations, the Reynolds number is fixed to be 10, and the pressures at the entrance and outlet are set to be $p_{in} = 1.1$ and $p_{out} = 1.0$. The present non-equilibrium extrapolation scheme, Eq.(20), is used to the entrance and outlet for the pressure boundary, and the scheme Eq.(21) is used at the top and bottom plates for the velocity boundary. In simulations, the criterion used for steady state is

$$\sum_{ij} \left| u_{ij}^{(n)} - u_{ij}^{(n-100)} \right| / \sum_{ij} \left| u_{ij}^{(n)} \right| \le 1.0 \times 10^{-9}, \tag{23}$$

where $u_{ij}^n = u(x_i, y_j, n\Delta t)$, and the summation is taken over the whole system.

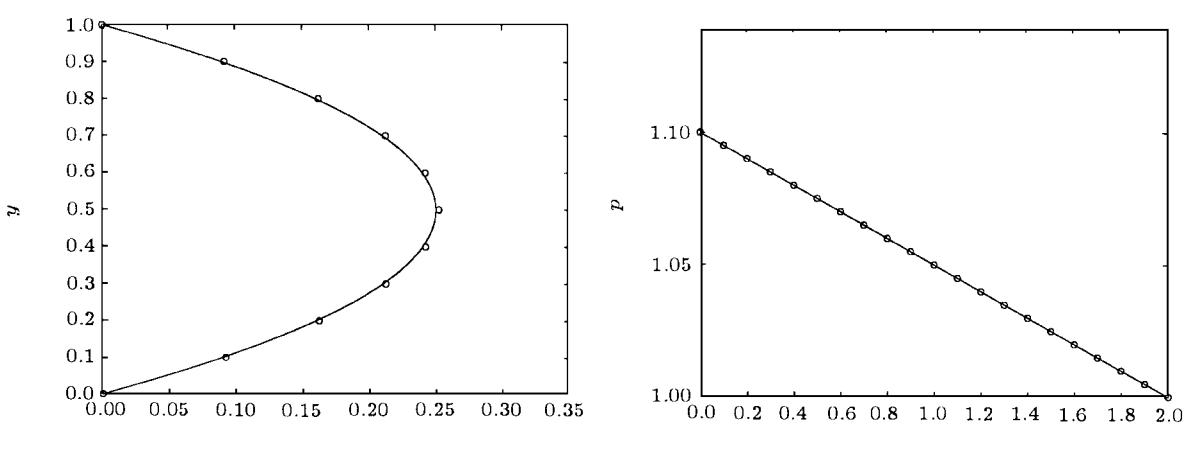

Fig.2. Velocity and pressure profiles for the Poiseuille flow ($\omega = 0.9, \Delta x = 0.1$). The symbols and solid lines represent the LBM and analytical solutions, respectively.

It is found that the flow reaches its steady state for all cases considered, and at the steady state, the horizontal velocity component u is uniform along the x-direction. The maximum absolute value of the vertical velocity component v is of the order of 10^{-11}. The pressure at the steady state is found to be uniform along the y-direction, and is linear along the x-direction. The profiles of velocity u and pressure are plotted in Fig.2 for $\omega = 0.9$ and $\Delta x = 0.1$. As shown, the lattice Boltzmann solutions are in good agreement with the analytical solutions.

Accuracy is studied by measuring the convergence rate of the relative global error as the lattice spacing changes, where the relative global error is defined as

$$E = \frac{\sqrt{\sum (u - u_e)^2 + (v - v_e)^2}}{\sqrt{\sum u_e^2}}, \tag{24}$$

where (u, v) is the numerical solution and (u_e, v_e) is the analytical solution. In Fig.3, the relative global errors are plotted logarithmically as functions of the lattice spacing. The slopes of the least-squares fits are about 2.0002, 2.0001 and 2.0002 for $\omega = 0.9$, 1.1 and 1.7, respectively. This indicates that the accuracy of the present boundary conditions is really of second order in space for the Poiseuille flow.

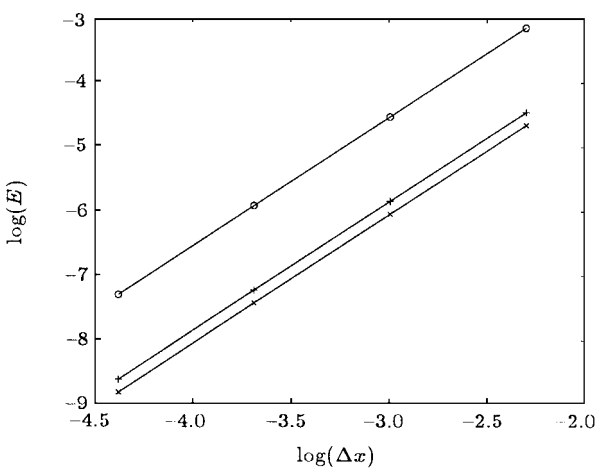

Fig.3. Relative error for the Poiseuille flow: $+, \omega = 0.9$; $\times, \omega = 1.1$; $\circ, \omega = 1.7$. The solid lines represent the least-squares fits. The slopes of the lines are 2.0000(+), 2.0001(×) and 2.0002 (∘), respectively.

4.2. Porous plate flow

The second test problem is the channel porous plate flow. In this flow, the upper plate moves with a constant velocity, u_0, and a constant normal flow is injected with a velocity v_0 through the fixed bottom plate and is withdrawn at the same rate from the upper plate. This flow models a fluid being sheared between two porous plates, through which an identical fluid is injected normal to the shearing direction. The problem provides a more general Dirichlet boundary condition, and can be used to test the ability of a boundary treatment.

In a steady state, the porous plate flow has the following analytical solution[14]

$$u_e = u_0 \left(\frac{e^{Re(y/L)} - 1}{e^{Re} - 1} \right), \tag{25}$$

where L is the channel width and the Reynolds number is defined as $Re = Lv_0/\nu$. There is a boundary layer near the moving top plate for this flow, and the thickness of the boundary layer decreases exponentially as Re increases. In simulations, the flow domain is set to be $0 \le x \le 2.0$, $0 \le y \le 1.0$. The constant velocity of the upper plate and the normal injection velocity are set to be $u_0 = v_0 = 0.1$, and the Reynolds number is chosen to be $Re = 5.0$. The present scheme for the velocity boundary, Eq.(21), is applied to the top and bottom plates, and the periodic boundary condition is applied to the inlet and exit.

In all cases, the flow reaches its steady state after a number of iterations. It is found that in the steady state, the velocity u is indeed uniform along the channel for each case. In Fig.4, the profiles of numerical results are plotted, as well as the analytical solutions, for $\omega = 0.9$ and $\Delta x = 0.05$. As is shown, the LBM results agree well with the analytical solutions.

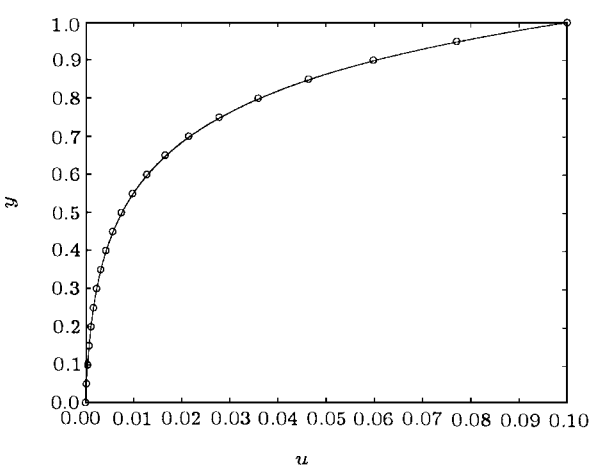

Fig.4. Velocity profiles for the porous plate flow ($\omega = 0.9, \Delta x = 0.05$). The symbols and solid lines represent the LBM and analytical solutions, respectively.

The convergence rate is studied based on the relative L_2 norm error in the velocity field, which is defined as

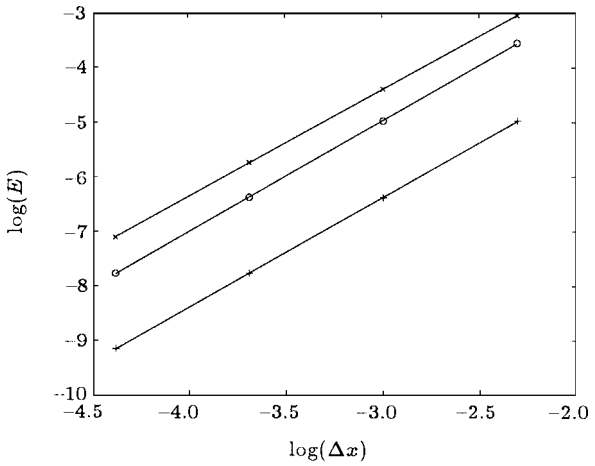

Fig.5. Relative error for the porous plate flow: $\circ, \omega = 0.9$; $+, \omega = 1.1$; $\times, \omega = 1.7$. The solid lines represent the least-squares fits. The slopes of the lines are 2.0288 ($\circ$), 2.0074 ($+$), and 1.9532 ($\times$), respectively.

$$E = \frac{\sqrt{\sum (u - u_e)^2}}{\sqrt{\sum u_e^2}}, \tag{26}$$

where u is the LBM solution, and the summation is taken over the entire domain. The errors are plotted logarithmically in Fig.5. It is found that the slopes of the least-square fits are 2.0288, 2.0074 and 1.9532 for $\omega = 0.9$, 1.1 and 1.7, respectively, indicating the second-order accuracy of the present scheme for the velocity boundary condition.

4.3. Oscillating plate flow

The oscillating plate problem is defined in the region $0 \le x, y \le 1.0$ under a periodic boundary condition at the entrance and exit. The bottom plate is kept stationary, and the top plate oscillates horizontally with a constant frequency, i.e. $u = \cos(\Omega t)$, where Ω is the oscillation frequency. The analytical solution of this oscillating plate problem has the following form

$$u_e = 2\frac{A\left[a\cos(\Omega t) - b\sin(\Omega t)\right] + B\left[a\sin(\Omega t) + b\cos(\Omega t)\right]}{\cosh(2St^*) - \cos(2St^*)}, \tag{27}$$

where $A = \cosh y^* \sin y^*$, $B = \cos y^* \sinh y^*$, $a = \cosh St^* \sin St^*$, $b = \cos St^* \sinh St^*$, with $St^* = St/\sqrt{2}$, $y^* = ySt^*$. Here St is the Stokes number defined as

$$St = \sqrt{\Omega/\nu}. \tag{28}$$

The Stokes number is an important parameter for the oscillating flow; it is in fact the ratio of the channel width to the thickness of the Stokes layer $\sqrt{\nu/\Omega}$.

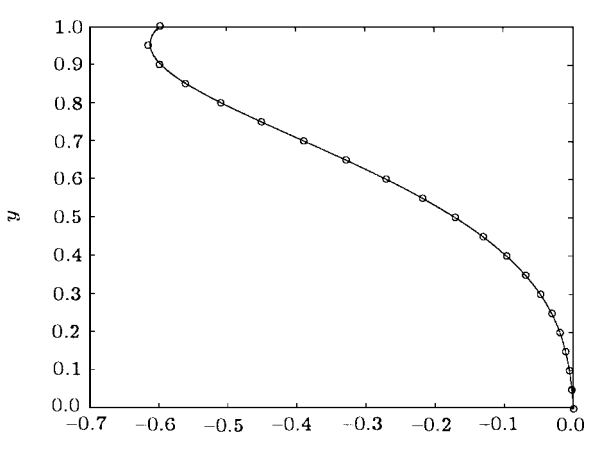

Fig.6. Velocity profiles for the oscillating plate flow at $t = 20.37037$ ($\omega = 0.9, \Delta x = 0.05$). The symbols and solid lines represent the LBM and analytical solutions, respectively.

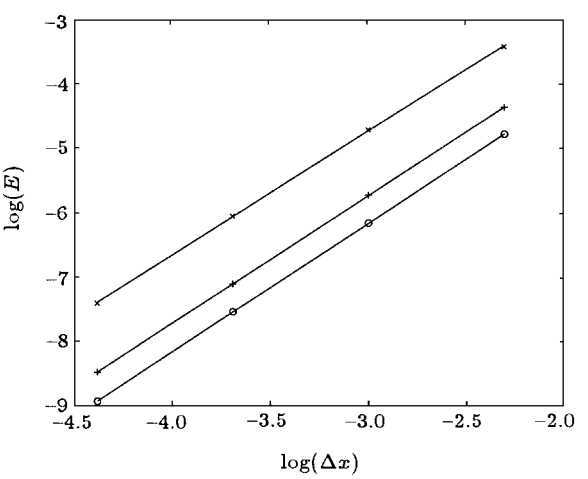

Fig.7. Relative errors for oscillation plate flow: $\circ, \omega = 0.9$; $+, \omega = 1.1$; $\times, \omega = 1.7$. The solid lines represent the least-squares fits. The slopes of the lines are 1.9940 ($\circ$), 1.9792 ($+$) and 1.9177 ($\times$), respectively.

Simulations are carried out using $\nu = 0.1$ and $\Omega = 2.0$. In simulations, the periodic boundary condition is applied to the entrance and exit, and the velocity boundary Eq.(21) is applied to the top and bottom plates. It is found that, each time, the velocity component u is uniform along the x-direction. The profiles of u in the case of $\omega = 0.9$ and $\Delta x = 0.05$ are plotted in Fig.6 together with the analytical solutions at time $t = 20.37037$. Excellent agreement is observed

between the LBM and the analytical solutions for this unsteady flow. The relative global errors are plotted logarithmically in Fig.7. The slopes of the least-square fits are 1.9940, 1.9792 and 1.9177 for $\omega = 0.9, 1.1$ and 1.7, respectively. Second-order accuracy of the present velocity boundary condition is clearly shown.

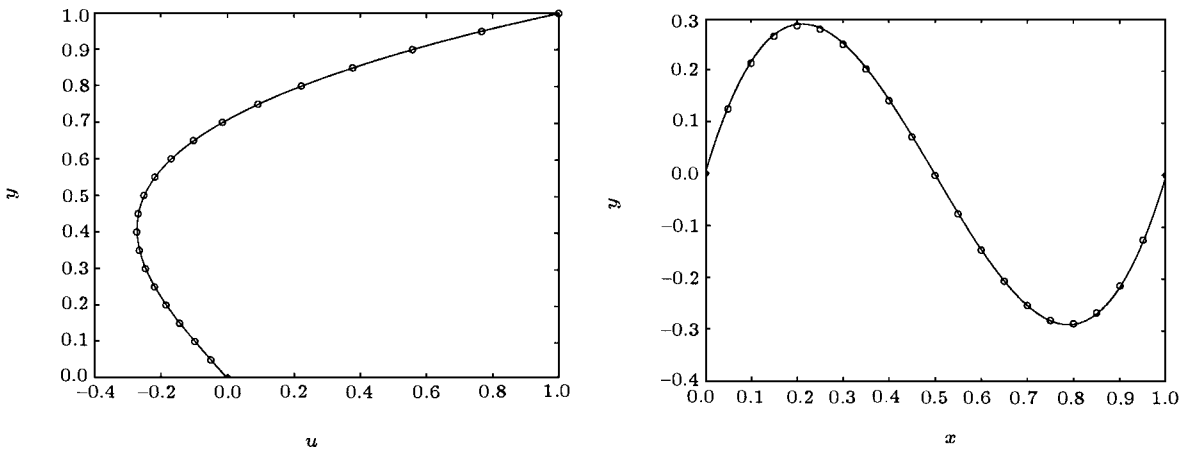

Fig.8. Velocity profiles for the driven cavity flow across the cavity centre ($\omega = 0.8, \Delta x = 0.05$). The symbols and solid lines represent the LBM and analytical solutions, respectively.

4.4. Cavity flow with analytical solution

The last test problem is the modified cavity flow, first proposed by Shin *et al.*[20]. The computation region is defined by $0 \leq x, y \leq 1.0$. A shear flow is imposed on the top wall with the following velocity profile

$$u = 16x^2(1-x)^2. \tag{29}$$

If the flow is exposed to a body force $\boldsymbol{F} = (F_1, F_2)$ defined by

$$\begin{aligned} F_1 =& 0, \\ F_2 =& 8\nu \left[24M(x) + 2m'(x)n''(y) + m'''(x)n(y)\right] \\ &+ 64\left[M_2(x)N(y) - n(y)n'(y)M_1(x)\right], \end{aligned} \tag{30}$$

where $m(x) = x^2(1-x)^2$, $n(y) = y^2(y^2-1)$, $M(x) = \int m(x)\mathrm{d}x$, $M_1(x) = m(x)m''(x) - (m'(x))^2$, $M_2(x) = \int mx(x)m'(x)\mathrm{d}x$, and $N(y) = n(y)n'''(y) - n'(y)n''(y)$. This driven cavity flow has a time-independent analytical solution

$$\begin{aligned} u_{\text{exact}} =& 8u_0 m(x/H)n'(y/H), \\ v_{\text{exact}} =& -8u_0 m'(x/H)n(y/H). \end{aligned} \tag{31}$$

In simulations, the kinematic viscosity ν is set to be 0.1, and the velocity at the boundaries is specified by evaluating the analytical solution. The present non-equilibrium extrapolation scheme for velocity boundary condition, Eq.(21), is applied to the four boundaries. In simulations, it is found that the flow reaches its final steady state for each case. In Fig.8, the profiles of the velocity across the cavity centre are plotted together with the analytical solutions in the case of $\omega = 1.1$ and $\Delta x = 0.05$. Excellent agreement is observed between the simulation results and the analytical solutions. In Fig.9, numerical errors are plotted logarithmically, where the error is defined as

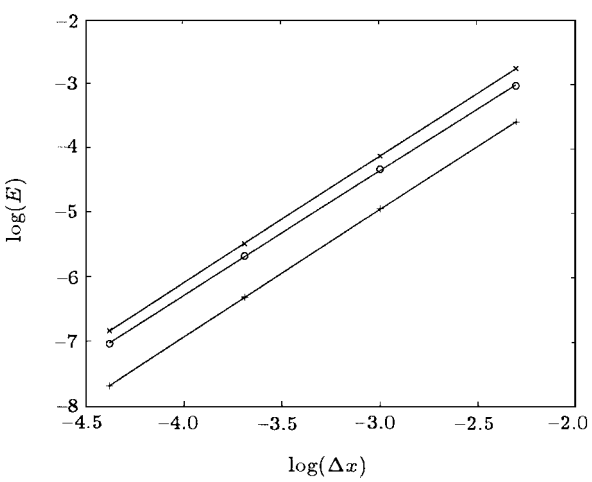

Fig.9. Relative errors for the driven cavity flow: $\circ, \omega = 0.8$; $+, \omega = 1.1$; $\times, \omega = 1.7$. The solid lines represent the least-squares fits. The slopes of the lines are 1.9340 ($\circ$), 1.9749 ($+$) and 1.9643 ($\times$), respectively.

$$E = \frac{\sqrt{\sum (u-u_e)^2 + (v-v_e)^2}}{\sqrt{\sum u_e^2 + v_e^2}}, \tag{32}$$

where the summation is taken over the whole domain. The slopes of the least-square fits are 1,9340, 1.9749

and 1.9643 for $\omega = 0.8$, 1.1 and 1.7, respectively. Quadratic convergence is clearly seen for the present velocity boundary condition.

4.5. Numerical stability comparison

For the LBM, the numerical stability depends on the relaxation time τ, the Mach number of the flow, and the size of the underlying lattice in use. In Chen's extrapolation boundary conditions,[18] an additional layer outside the physical boundary is needed, and the distribution functions at the node lying on the additional layer is determined from the distribution functions at the neighbouring boundary node and fluid node based on a second-order extrapolation scheme. Under the present boundary conditions, only first-order extrapolation is needed. It is well understood that the numerical stability of a lower-order extrapolation scheme is usually better than that of higher-order schemes. Therefore, it is expected that the present boundary conditions have better-behaved stability characteristics than Chen's extrapolation schemes.

To illustrate this point, we have applied the present schemes and Chen's schemes to the Poiseuille flow driven by a constant gradient. The geometry and parameters of the flow are set in the same way as used in Subsection A. We measured the maximum and minimum values of the relaxation time τ ($\tau_{\max}$ and $\tau_{\min}$) at which the computation is still stable. In Fig.10, $\tau_{\min}$ and $\tau_{\max}$ are plotted as functions of the lattice spacing. It is well known that the numerical stability of the LBM usually becomes very poor as τ approaches 0.5. It is found that $\tau_{\min} > 0.7$ for Chen's schemes in all cases considered here, while $\tau_{\min} \leq 0.51$ for the present boundary conditions. This indicates that the numerical stability of the present schemes is greatly improved, compared with Chen's schemes. At the same time, it is found that the value of $\tau_{\max}$ for the present schemes is always greater that that for Chen's schemes. These facts show that the stable region of the present schemes is much larger than that of Chen's schemes. A similar behaviour is also observed in the simulations of other test problems.

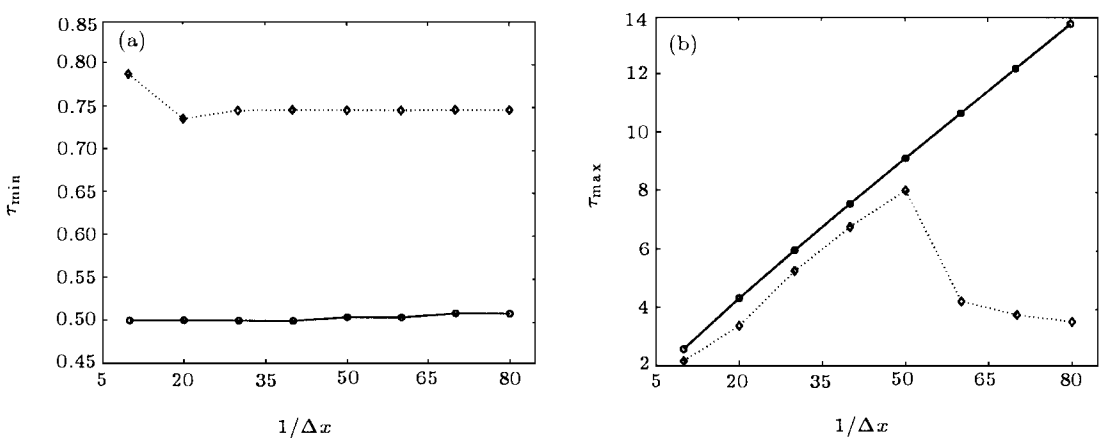

Fig.10. Minimum and maximum values of τ usable for the present schemes and Chen's schemes in simulation of the Poiseuille flow: (a) minimum value; (b) maximum value; Solid, present method; dotted, Chen's method.[18]

5. Conclusions

In this paper we have proposed a new method to implement boundary conditions in the LBM. The basic idea is to decompose the distribution function at the boundary node into its equilibrium and non-equilibrium parts. The non-equilibrium part is approximated with the non-equilibrium distribution function at the neighbouring fluid node. Schemes for pressure and velocity boundary conditions based on this method are proven to be of second-order accuracy. Numerical tests are carried out, including two-dimensional Poiseuille flow, porous plate flow, oscillating plate flow, and driven cavity flow. Simulation results indicate that the LBM solutions using the present boundary schemes are in excellent agreement with the analytical solutions. Second-order convergence is also observed for the present schemes. It is also shown that the numerical stability of the present schemes is much better than that of Chen's extrapolation schemes.

Like the original extrapolation method proposed in Ref.[18], the present non-equilibrium extrapolation method does not need any *ad hoc* assumptions about the incoming distributions, and can be easily extended to design schemes for other boundary conditions, such as thermal boundary, velocity flux and temperature boundary. Furthermore, the proposed method needs no additional layer beyond the physical boundary layer, and thus has better memory efficiency, and is more suitable in handling flows in complex geometry.

In conclusion, we have proposed a new method for the implementation of boundary conditions in the LBM. Schemes for pressure and velocity boundaries are given based on this method, which are shown to be of second-order accuracy, and have better numerical stability, compared with the original extrapolation schemes.

Acknowledgments

Z. Guo is grateful to Professor Y.H. Qian and Professor H.P. Fang for helpful discussions on the BICCP Workshop on the Lattice-Based Method.

References

[1] Sun C 1998 *Phys. Rev.* E **58** 7283
[2] Qian Y 1993 *J. Sci. Comput.* **8** 231
[3] Li H B *et al* 2000 *Acta Phys. Sin.* **49** 392 (in Chinese)
[4] Feng S and Michihisa T 2001 *Acta Phys. Sin.* **50** 1006 (in Chinese)
[5] Shan X and Chen H 1993 *Phys. Rev.* E **47** 1815
[6] Fang H P *et al* 2000 *Chin. Phys.* **49** 515
[7] Qian Y *et al* 1995 *Ann. Rev. Comp. Phys.* **3** 195
[8] Chen S and Doolen G 1998 *Ann. Rev. Fluid Mech.* **30** 329.
[9] Gallivan M A *et al* 1997 *Int. J. Numer. Methods Fluids* **25** 249
[10] Zou Q and He X 1995 *Phys. Fluids* **9** 1591
[11] D'Humeiéres D and Lallemand P 1987 *Complex Syst.* **1** 599
[12] Ziegler D P 1993 *J. Stat. Phys.* **71** 1171
[13] Cornubert R *et al* 1991 *Physica* D **47** 241
[14] Noble D R *et al* 1995 *Phys. Fluids* **7** 203
[15] Skordos P A 1993 *Phys. Rev.* E **48** 4823
[16] Maier R S *et al* 1996 *Phys. Fluids* **8** 1788
[17] Inamuro T *et al* 1995 *Phys. Fluids* **7** 2928
[18] Chen S *et al* 1996 *Phys. Fluids* **8** 2527
[19] Guo Z *et al* 2000 *J. Comput. Phys.* **165** 288
[20] Shin T M *et al* 1989 *Int. J. Numer. Methods Fluids* **9** 193